





Tuning the energy landscape of CaTiO_3 into that of antiferroelectric PbZrO_3

Huazhang Zhang ^{1,2,*}, Chih-Hsuan Chao,¹ Louis Bastogne ¹, Alireza Sasani ¹ and Philippe Ghosez ^{1,†}

¹Theoretical Materials Physics, Q-MAT, CESAM, Université de Lige, B-4000 Sart-Tilman, Belgium

²Department of Physics, School of Science, Wuhan University of Technology, Wuhan 430070, People's Republic of China



(Received 21 July 2023; revised 4 October 2023; accepted 4 October 2023; published 20 October 2023)

PbZrO_3 and CaTiO_3 appear *a priori* as similar ABO_3 oxide perovskites with very close tolerance factors. Amazingly, they show, however, significantly distinct properties: while PbZrO_3 is a prototypical antiferroelectric, CaTiO_3 is not. Here, we investigate the microscopic origin of their different behaviors. From the comparison of the harmonic and anharmonic interatomic force constants, we highlight that the key differences are in their A-O interactions. Then, specifically tuning the harmonic and anharmonic coefficients of these interactions, we show that it is possible to make the energy landscape of CaTiO_3 very similar to that of PbZrO_3 .

DOI: [10.1103/PhysRevB.108.L140304](https://doi.org/10.1103/PhysRevB.108.L140304)

Introduction. Antiferroelectric (AFE) materials refer to a class of crystals that are naturally in a nonpolar phase and can be switched into a polar phase under the application of an external electric field [1,2]. Macroscopically, AFEs show double hysteresis loops of polarization versus electric field [3]. This specific feature is very appealing for applications in energy storage and electrocaloric cooling [4–8], which has recently fueled a renewal of interest for antiferroelectricity. However, there are only a few materials known to be AFE, and most of them belong to the family of oxide perovskites, such as PbZrO_3 (PZO) [9,10], PbHfO_3 [11], NaNbO_3 [12], and AgNbO_3 [13]. Clarifying further the underlying principles that make a compound like PZO an antiferroelectric, while many other perovskites like CaTiO_3 (CTO) are not, therefore appears as a natural and timely step forward in the rational search and design of new AFE materials.

Among the large number of oxide perovskites, CTO show a tolerance factor, t , very close to that of PZO: $t(\text{PZO}) = 0.9701$ (resp. 0.940) and $t(\text{CTO}) = 0.9730$ (resp. 0.946) using Shannon atomic radii [14,15] (resp. bond valence parameters [16]). This suggests that both compounds should exhibit very similar behaviors. Amazingly, this is, however, not the case. Both materials share the same $Pm\bar{3}m$ structure at high temperatures but as the temperature decreases, they pass through a distinct sequence of intermediate phases and exhibit different room-temperature (RT) and ground-state (GS) structures.

In PZO, the RT phase is $Pbam$ and shows double hysteresis loops classifying it as AFE [17,18]. This phase was thought for a long time to also be the GS structure, but this has been questioned recently after the theoretical discovery of a $Pnma$ 80-atom phase [19] and a ferrielectric $Ima2$ phase [20], which are slightly lower in energy than $Pbam$ (energy difference around 1 meV/f.u.). These interesting new findings do not question the well-attested AFE character of the $Pbam$ phase at room temperature but highlight a very flat energy landscape

with various close energy minima in line with the existence of an easy path to rotate dipoles in an electric field and reach a polar phase from the $Pbam$ state. The fact that the ground state could be ferro or ferrielectric would not be unusual since the RT phase of NaNbO_3 is also known to be AFE while its GS is ferroelectric.

In CTO, the RT and GS phase is instead $Pnma$, as in many perovskites with $t < 1$ [21]. Although this phase also contains antipolar motions of the A cations, arising from a trilinear coupling with oxygen rotations and tilts, it is not known to be AFE. At the macroscopic level, CTO is a regular dielectric showing a linear evolution of its polarization in an electric field. It manifests an eventual increase of dielectric constant at low-temperature, questioning a potential incipient ferroelectric character [22], but do not show any tendency to double hysteresis loops. Considering the similarity in tolerance factor of these two oxide perovskites, a natural question arises: why is PZO AFE while CTO is not?

Previous studies have shown that there is in fact a significant difference between PZO and CTO in their electronic structure. In PZO, there are significant hybridizations between the Pb 6s and O 2p states [23], while in CTO the Ca-O interaction is essentially ionic [24]. Although certainly pointing in the right direction, only highlighting this fact seems a bit short to answer the above question convincingly, because the AFE is a complex property directly linked to the lattice so that the connection is not so straightforward.

At the lattice-dynamics level, a number of studies have been devoted to understanding the $Pbam$ phase of PZO. Tagantsev *et al.* [25] proposed that the antiferroelectric $Pbam$ state is a “missed” incommensurate phase, and its condensation is driven by the softening of a single polar mode via flexoelectric coupling. Independently, Hlinka *et al.* [26] and Íñiguez *et al.* [27] pointed out that the octahedral rotations and a trilinear coupling of distortions play the key role in stabilization of the $Pbam$ state. Patel *et al.* [28] reported that a bilinear coupling between the local dipoles and octahedral rotations is another important ingredient. Recently, Shapovalov and Stengel [29] reformulated the problem in terms of an essential

*Corresponding author: hzhang@uliege.be

†Corresponding author: philippe.ghosez@uliege.be

rotopolar coupling between polarization, rotation, and rotation gradients, merging some of the previous thoughts into a single physical mechanism. Although a unified understanding for the *Pbam* ground state is emerging, it is still unclear why the same mechanism is not at play in similar perovskite such as CTO.

In addition, AFE properties rely not only on the specific nonpolar ground state but also on the ability of switching from the nonpolar to a polar phase under electric field, which means that some flatness of the energy surface is also very crucial. Therefore, to achieve better understanding of the mechanism behind antiferroelectricity, it is necessary to expand the focus from a specific phase to a wider region of the energy landscape.

Sampling of the Born-Oppenheimer potential energy surface (PES) of each individual material can be achieved from first-principles calculations but is not sufficient to unveil the relevant physics. Starting from the reference cubic structure, it is also possible to make a Taylor expansion of the PES in terms of individual atomic displacements and macroscopic strains, and to determine all coefficients from first-principles data in a so-called second-principles approach. In this expansion, individual coefficients are connected to specific physical quantities such as interatomic force constants (IFC) in real space, elastic constant, strain-phonon couplings, etc. These can then be compared from one material to another in order to trace back in a more transparent way which specific interactions are responsible for the key changes in the energy landscape.

In the present work, we explore the PES of PZO and CTO by comparing their phonon dispersion curves in the reference cubic structure and the energies of various potentially metastable low-energy phases. We then compare their harmonic and anharmonic IFCs and identify that key differences in the A-O interactions (i.e., Pb-O in PZO and Ca-O in CTO), at both harmonic and anharmonic levels, are crucial to explain the distinct energy landscapes of PZO and CTO. Tuning then just these A-O interactions, we show that it is possible to recover in CTO an energy landscape very similar to that observed in PZO.

Methods. The first-principles calculations have been performed in the framework of density functional theory (DFT) using the ABINIT package [30–33] and a planewave-pseudopotential approach. The calculations were based on the generalized gradient approximation and norm conserving pseudopotentials [34,35]. For the calculations of PZO, we used the revised Perdew-Burke-Ernzerh functional for solids (PBEsol) [36]. The energy cutoff for the plane-wave expansion was 60 Ha, and the Brillouin zone sampling was equivalent or denser to a $6 \times 6 \times 6$ k -point grid for the five-atom perovskite cell. For the calculations of CTO, we used the Wu-Cohen (WC) parametrization for the exchange-correlation potential [37] in order to maintain consistency with a previous study [38]. We checked that PBEsol and Wu-Cohen GGA functionals provide comparable results (Fig. S1 [39]) and that our conclusions are not affected by this specific technical choice. The plane wave expansion was cut-off at 40 Ha, and k -point grids were equivalent to an $8 \times 8 \times 8$ with respect to the five-atom perovskite cubic unit cell. The electronic self-consistent cycles were converged until the potential residual is smaller than 10^{-18} Ha.

Structural relaxations were performed based on the Broyden-Fletcher-Goldfarb-Shanno (BFGS) minimization algorithm, using the convergence criteria of 10^{-6} Ha/Bohr for the forces and 10^{-8} Ha/Bohr³ for the stresses. The second-order derivatives of energy and the related properties (e.g., phonon frequencies, Born effective charges, harmonic interatomic force constants, etc.) were calculated according to density functional perturbation theory (DFPT) [40].

The Taylor expansion of the PES, around the reference cubic structure, in terms of individual atomic displacements and homogeneous strains, together with the determination of all parameters from first-principles data, was realized with MULTIBINIT [30], implementing the scheme proposed by Wojdeł *et al.* [41,42]. In this scheme, the energy includes harmonic and anharmonic contributions in terms of atomic displacements, strains, and their couplings. At the harmonic level, the coefficients are exactly those directly computed from DFPT. At the anharmonic level, the number of terms become gigantic; to keep the approach tractable, the most relevant terms are selected and their coefficient are fitted in order to reproduce the energies, forces, and stresses computed from DFT for a set of configurations properly sampling the PES. Here, we used the model previously developed by Schmitt for CTO [38] and fitted a similar model for PZO. BFGS structural relaxations were then performed using these second-principles models, with the convergence criteria of 10^{-4} Ha/Bohr for the forces and 10^{-6} Ha/Bohr³ for the stresses. At the second-principles level, phonon dispersion curves were calculated based on the finite difference method, using PHONOPY [43] to analyze the force set produced by MULTIBINIT.

Typically, all energies reported for PZO have been double checked at the DFT level while the energy landscapes of CTO and modified CTO have been obtained at the second-principles level [38].

Results and Discussion. We first compare the curvatures of the PES around the cubic reference structure (RS) in PZO and CTO from the analysis of their phonon dispersion curves in the cubic phase. PZO displays phonon instabilities at all high-symmetry q points, i.e., Γ , X , M , and R [Fig. 1(a)]. The in-phase and antiphase rotations of oxygen octahedra at M and R points show the strongest instabilities (177.9i and 183.6i cm⁻¹), followed by the ferroelectric instabilities at Γ point (135.7i cm⁻¹). PZO also exhibits other unstable modes at M and R points, which are related to antipolar motions. In contrast to PZO, CTO possesses fewer unstable branches [Fig. 1(b)]. The strongest instabilities are the in-phase and antiphase oxygen octahedra rotations at M and R (198.3i and 209.3i cm⁻¹). The polar modes at Γ are less unstable (139.3i cm⁻¹), whereas the antipolar modes at X , M , and R , which are unstable in PZO, are all stable in CTO.

To explore the energy minima and saddle points of the PES, away from the RS, we performed structural relaxations of various (meta)stable phases produced by the condensation of distinct soft modes. The energy gains of these different phases with respect to the cubic reference structure, obtained by fully relaxing the atomic positions and cell parameters, are plotted in Fig. 1, when ordered according to their decreasing amplitude of energy gains either in PZO [Fig. 1(c)] or in CTO [Fig. 1(d)]. In PZO, we see a rather smooth and

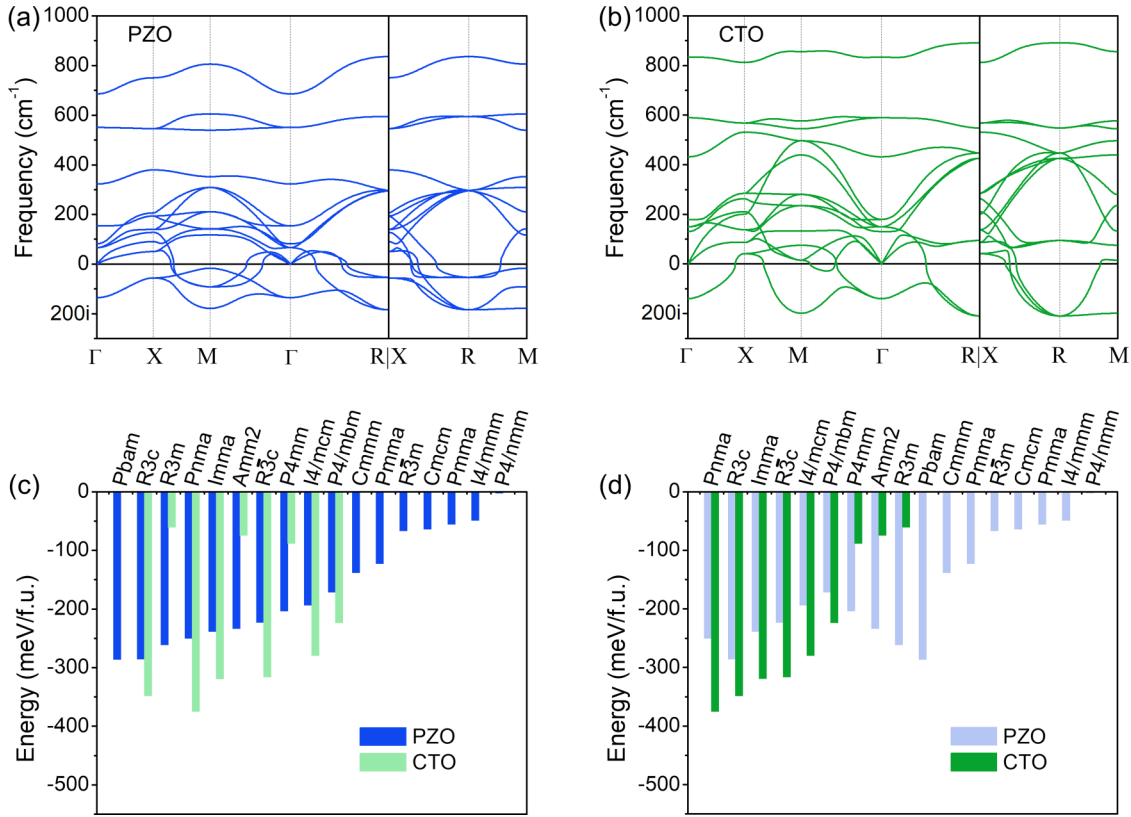


FIG. 1. Comparisons of the energy landscapes of PZO and CTO. [(a), (b)] Phonon dispersion curves of the reference cubic phase for PZO and CTO, respectively. [(c), (d)] Energies of various (meta)stable phases of PZO and CTO, respect to the cubic phase taken as energy reference in each case. Phases are ordered according to decreasing energy gains either in PZO [panel (c)] or CTO [panel (d)].

continuous evolution of energy gains in the different phases associated with the condensation of the most unstable modes at Γ ($P4mm$, $Amm2$, $R3m$), M ($P4/mbm$), and R ($I4/mcm$, $Imma$, $R\bar{3}c$) points. In CTO, the energy gains of pure polar phases ($P4mm$, $Amm2$, $R3m$) are notably smaller than that of other phases, and there is a gap, without any metastable phase, between these polar phases and the rotational phases ($P4/mbm$, $I4/mcm$, $Imma$, $R\bar{3}c$). In addition, since CTO has no antipolar instabilities at X, M, and R points, the corresponding local minima ($Pmma$, $Cmcm$, $Cmmm$, $P4/nmm$, $I4/mmm$, $R\bar{3}m$) disappear on the PES of CTO. We checked explicitly the potential stability of these phases and it turns out that they relax back to the RS. Also, we did a full relaxation starting from $Pbam$ phase in CTO and the system evolves toward a final $Imma$ phase, in which the antipolar Σ mode is suppressed. All these characteristics of the energy sequence are preserved in fixed-cell relaxations (Fig. S2 [39]), indicating that the strains do not play a significant role in these two materials. Overall, the PES of PZO show much more minima or saddle points which are close in energy, providing more opportunities for low energy paths during transitions between different phases. Comparably, the PES of CTO is much more rugged with less energy minima at more distinct energy scales.

If we consider the criteria for antiferroelectricity, it appears that PZO and CTO possess both nonpolar ground state, $Pbam$ and $Pnma$, and a polar $R3c$ phase whose energy is only slightly higher than the ground states. The energy difference between $Pbam$ and $R3c$ is less than 1 meV/f.u. in PZO, and

the difference between $Pnma$ and $R3c$ is about 26 meV/f.u. in CTO. Although the latter is a bit larger, the electric field required for the $R3c$ phase to become thermodynamically more stable than $Pnma$ in CTO is of the order of 1.2×10^8 V/m, which remains accessible.

Beyond the proximity of a polar phase with the nonpolar ground state, another key requirement for AFE behavior is that the energy barrier between these phases needs to be sufficiently low, which seems to be more crucial in explaining the distinct behaviors of PZO and CTO. In PZO, the series of low energy phases involving either polar, antipolar, and rotational modes gives a hint that the phase transition would be much more easy via hopping between these local minima. These characteristics of PES are exactly what is lacking in CTO.

We now turn to seek and identify the key interactions responsible for the main differences between PZO and CTO. At first, we notice that atomic mass differences do not play a major role in this context (Fig. S3 [39]). We thus focus on the interatomic force constants (IFCs), especially those whose interatomic distance is not larger than the length of the unit cell. In Table I, we have used the conventional definition of the interatomic force constant, given by $C_{\alpha,\beta}(l\kappa, l'\kappa') = -F_{\alpha}(l\kappa)/\Delta\tau_{\beta}(l'\kappa')$ [44], which relates the forces $F_{\alpha}(l\kappa)$ acting on atom κ in cell l along direction α to the displacement $\Delta\tau_{\beta}(l'\kappa')$ of atom κ' in cell l' along direction β . For $l\kappa \neq l'\kappa'$, the IFC can be interpreted as the opposite of the stiffness constant of a virtual spring bridging the two atoms. So, a negative value of IFC means that the interaction is

TABLE I. Values (Ha/Bohr²) of the harmonic interatomic force constants in real space in local coordinates for distinct nearest-neighbor pairs of atoms in the reference cubic structure. The symbols \parallel and \perp refer to the longitudinal and transverse components, respectively. Negative values correspond to stable interactions (i.e., generating a restoring force). A comparison of our results with previous results in the literature relying on distinct functionals is also provided.

		PZO	PZO [44]	CTO	CTO [45]
A-O	\parallel	+0.0124	+0.0139	+0.0110	+0.0108
	\perp_1	-0.0049		-0.0055	-0.0055
	\perp_2 (zz)	-0.0099	-0.0103	-0.0112	-0.0116
B-O	\parallel	-0.0549	-0.0687	-0.0369	-0.0382
	\perp	-0.0104	-0.0100	-0.0184	-0.0184
A-B	\parallel	-0.0271	-0.0271	-0.0273	-0.0266
	\perp	+0.0138	+0.0145	+0.0144	+0.0150
A-A'	\parallel	-0.0097	-0.0094	-0.0086	-0.0085
	\perp	+0.0052	+0.0056	+0.0037	+0.0040
B-B'	\parallel	-0.0508	-0.0499	-0.0814	-0.0788
	\perp	+0.0049	+0.0054	+0.0089	+0.0084

stable (tends to recover under stretch or compression), and a positive value means it is unstable (could not maintain a stable interatomic distance). The on-site force constants ($l\kappa = l'\kappa'$) in Table II follow the definition $C_{\alpha,\beta}(l\kappa, l\kappa) = -\sum_{l'\kappa' (\neq l\kappa)} C_{\alpha,\beta}(l\kappa, l'\kappa')$ [44], and give the opposite indication as the IFCs, i.e., positive value of on-site force constant represents stability and negative value represents instability.

From Tables I and II, it appears that the signs of all IFCs and on-site force constants are the same in PZO and CTO, indicating that the two materials show similar stability from the local perspective. The A-O interaction is destabilizing (positive) along the longitudinal direction, A-A' is destabilizing (positive) along the transverse directions in both compounds, but both A-O (\parallel) and A-A' (\perp) are softer in PZO. Hence, there is more tendency in PZO than CTO for the A-O-A chain to form a short-long bond arrangement and the A-A-A chain to form a transverse wave. This observation is consistent with the analysis of the phonon dispersion curves showing that PZO has much more instabilities of polar/antipolar character than CTO. In line with their tolerance factor smaller than one, the B atom shows fewer instabilities compared to the A atom,

TABLE II. Values (Ha/Bohr²) of the on-site harmonic interatomic force constants in real space for distinct atoms in the reference cubic structure. Positive values correspond to stable interactions (i.e., generating a restoring force). A comparison of our results with previous results in the literature relying on distinct functionals is also provided.

		PZO	PZO [44]	CTO	CTO [45]
A	$xx = yy = zz$	+0.0163	+0.0129	+0.0267	+0.0269
B	$xx = yy = zz$	+0.2068	+0.2302	+0.2230	+0.2236
O	$xx = yy$	+0.0203	+0.0166	+0.0433	+0.0432
O	zz	+0.2454	+0.2758	+0.2623	+0.2624

which is manifested by the much larger on-site force constant of the B atom than that of the A atom, and the quite weak instability of B-B' (\perp) compared with the strong stability of B-B' (\parallel). Therefore, the key differences in the polar/antipolar modes and phases in PZO and CTO are very likely linked to the interactions involving the A atoms.

Relying on the previous analysis, we can then individually adjust the IFCs for each nearest neighbor atomic pair to investigate how this affects the phonon instabilities. In this way, we directly probe the effect of individual IFCs on specific modes. To facilitate comparison, we replaced certain interactions in CTO with their corresponding ones in PZO and examined whether the modified CTO model could recover the main features of PZO.

In Figs. 2(a) and 2(b), we examine the effect of the nearest A-O interactions. Amazingly, replacing only the nearest A-O interactions changes the phonon instabilities of CTO making them quite similar to PZO [Fig. 2(a)]. In particular, the antipolar modes at X, M, and R, which were initially stable, become unstable after modification [Fig. 2(b)]. Besides, the instability of the lowest phonon band is enhanced, especially the polar modes at the Γ point. Hence, this highlights that the A-O harmonic interaction is crucial for explaining the differences between CTO and PZO at the harmonic level.

We have also modified the harmonic IFCs of other nearest neighbor atomic pairs. However, unlike the modification of the nearest A-O interactions, altering these other harmonic IFCs has either a negligible effect on the phonon instabilities or does not result in a change of the phonon dispersions toward PZO (Fig. S4 [39]). Therefore, we conclude that, at the harmonic level, the A-O interaction is the key factor responsible for the distinct behavior of CTO and PZO.

It is now interesting to examine if the modifications of CTO at harmonic level are sufficient to also reproduce the energy gains of the (meta)stable phases of PZO. To properly disentangle the role played by harmonic and anharmonic interactions, we consider here an extreme case in which all the harmonic IFCs of CTO have been replaced by those of PZO, so that both materials are rigorously identical at the harmonic level. We refer to this artificial case as PZOhar + CTOanh and investigated the energy landscape in this specific case. Our findings [Fig. 2(c)] can be summarized as follows. First, it is now possible to relax a *Pbam* phase, and this *Pbam* phase exhibits the lowest energy. Second, due to the onset of the unstable antipolar modes at the harmonic level, the pure antipolar phases (*Pmma*, *Cmcm*, *Cmmm*, *P4/nmm*, *I4/mmm*, *R3m*) appear on the PES. Nonetheless, compared to PZO, the modified PES is still rugged since some phases show anomalously low energy, including the antiferroelectric *Pbam*, polar phases *R3c*, *Amm2*, *P4mm*, and the CTO ground state *Pnma*. We therefore conclude that difference at harmonic level between PZO and CTO is insufficient to account fully for the differences in the energy landscapes of both compounds.

Accordingly, we now turn to the search of the crucial differences in the anharmonic interactions. The over stabilization of polar phases on PZOhar + CTOanh suggests that the crucial anharmonic interactions should have the ability to eliminate this feature. We analyzed the energy contribution of each anharmonic term in the PZOhar + CTOanh model on

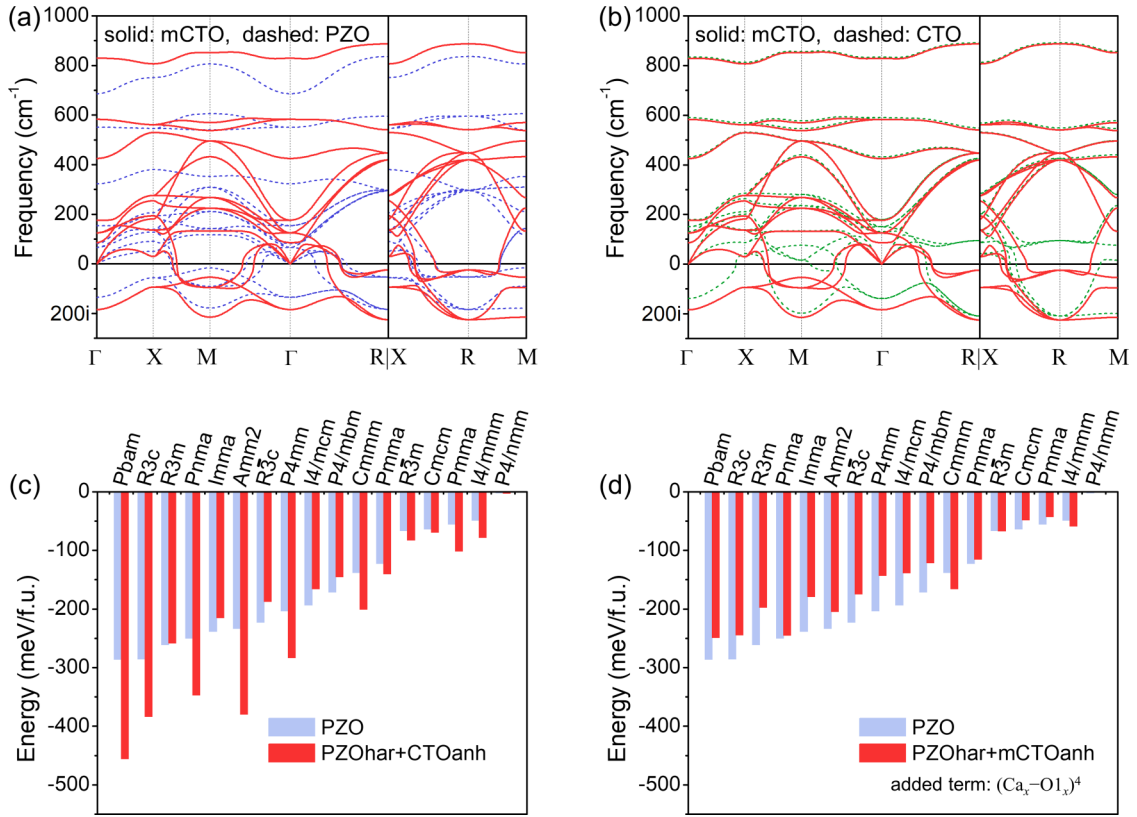


FIG. 2. Tuning CTO similar to PZO. [(a), (b)] Phonon dispersion curves of the cubic reference structure of a modified CTO model (mCTO, solid red curves), in which the nearest A-O CTO harmonic IFCs were replaced with the PZO ones, in comparison with the phonon dispersion curves of bare PZO and CTO (dashed curves), respectively. [(c), (d)] Comparison of the energy gains of distinct (meta)stable phases of PZO (light blue bars) with those of modified CTO models (red bars) combining (c) the harmonic part of PZO with the anharmonic part of CTO (PZOhar + CTOanh) and (d) including on top a symmetry adapted term $(\text{Ca}_x\text{-O1}_x)^4$ with a coefficient of $0.4259 \times 10^{-3} \text{ Ha/Bohr}^4$ similar to that in PZO.

the (meta)stable phases and identified a few candidate terms (Fig. S5 [39]). We examined the effects of tuning these anharmonic terms without, however, finding a way to reproduce a behavior similar to PZO (Fig. S6 [39]). It is therefore hard to conclude if the role of these terms is crucial.

Instead, it is also possible that the crucial term for realizing the PZO PES does not exist in our CTO model (limited to most relevant anharmonicities). To figure out the missed but crucial term, we compared the dominant anharmonic terms in CTO and PZO. We found that the term $(\text{A}_x\text{-O1}_x)^4$, which corresponds to an anharmonic interaction between A-O, contributes a large proportion in most phases in PZO, while this term does not appear in CTO. Relying on that, we investigated the effect of this term by adding it to the PZOhar + CTOanh model while simply keeping its value the same as in the PZO model. Intriguingly, adding this term now results in a similar trend of energy gains than in PZO (Fig. 2(d) and Fig. S7 [39]). It reduces the stability of all the metastable phases, particularly those anomalously low in energy. Although there is still some slight roughness, the energy gains are now much smoother than in the pristine CTO model and quite close to that of PZO. We can thus infer that this anharmonic term $(\text{A}_x\text{-O1}_x)^4$ is crucial for imitating the PZO energy landscape.

It is very interesting to observe that, at both the harmonic and the anharmonic levels, the key difference between PZO

and CTO appears located in the nearest A-O interactions. This allows us to make a clear link between the distinct electronic and dynamical properties of PZO and CTO previously mentioned. The Pb ion has a $6s^2$ lone pair, and the Pb-O bond in Pb-based perovskites is partially covalent [46,47]. There is a strong preference for the Pb ion to have a noncentrosymmetric coordination environment, because the hybridization between the Pb $6s$ and O $2p$ states gives rise to an additional driving force for the Pb to be off centering than the geometric factor (i.e., tolerance factor < 1). In contrast, the Ca-O bond in CTO is largely ionic [24]. The driving force is almost solely geometric, and therefore the off centering tendency of Ca in CTO is much weaker compared to that of the Pb in PZO. Thus, it can be seen that the distinct characters of the A-O bond and the differential behaviors of the A-O interactions are closely interrelated. From the present study, it is the difference in A-O interactions that dominantly explain the different PES between PZO and CTO.

Conclusion. To summarize, we have questioned why PZO is AFE while CTO is not, although both compounds exhibit very similar tolerance factors. Doing so, it appeared that not only their RT and GS phases are distinct but their whole energy landscapes show significantly different features. We highlighted that, already in their cubic reference structures, both compounds show significantly different phonon

dispersion curves, which has been specifically assigned to distinct first neighbor A-O harmonic interactions. We have shown that tuning the latter in CTO, allows to recover the dispersion curves of PZO but is not enough to reproduce its full energy landscape, which further requires also including anharmonic A-O corrections. It is known that, at the electronic level, the Pb-O bond in PZO is much more covalent than the Ca-O bond in CTO. Our work provides strong evidence that the simple renormalization of A-O harmonic and anharmonic interactions is the dominant factor explaining the different GS and energy landscape of both compounds.

Acknowledgments. This work was supported by the European Union's Horizon 2020 research and innovation program under Grant Agreement No. 964931 (TSAR) and by F.R.S.-FNRS Belgium under PDR Grant T.0107.20 (PROMOSPAN). H.Z. acknowledges the International Postdoctoral Exchange Fellowship (PC2020060) and the Research IPD-STEMA Program. C.H.C. acknowledges the AMIS Master Program and the EMMI. The authors acknowledge the use of the CECI supercomputer facilities funded by the F.R.S-FNRS (Grant No. 2.5020.1) and of the Tier-1 supercomputer of the Fédération Wallonie-Bruxelles funded by the Walloon Region (Grant No. 1117545).

- [1] K. M. Rabe, Antiferroelectricity in oxides a reexamination, in *Functional Metal Oxides New Science and Novel Applications*, edited by S. B. Ogale, T. V. Venkatesan, and M. G. Blamire (Wiley, 2013), pp. 221–244.
- [2] C. Kittel, Theory of antiferroelectric crystals, *Phys. Rev.* **82**, 729 (1951).
- [3] L. Jin, F. Li, and S. Zhang, Decoding the fingerprint of ferroelectric loops: Comprehension of the material properties and structures, *J. Am. Ceram. Soc.* **97**, 1 (2014).
- [4] X. Hao, J. Zhai, L. B. Kong, and Z. Xu, A comprehensive review on the progress of lead zirconate-based antiferroelectric materials, *Prog. Mater. Sci.* **63**, 1 (2014).
- [5] Z. Liu, T. Lu, J. Ye, G. Wang, X. Dong, R. Withers, and Y. Liu, Antiferroelectrics for energy storage applications: A review, *Adv. Mater. Technol.* **3**, 1800111 (2018).
- [6] Z. Yao, Z. Song, H. Hao, Z. Yu, M. Cao, S. Zhang, M. T. Lanagan, and H. Liu, Homogeneous/inhomogeneous-structured dielectrics and their energy-storage performances, *Adv. Mater.* **29**, 1601727 (2017).
- [7] A. S. Mischenko, Q. Zhang, J. F. Scott, R. W. Whatmore, and N. D. Mathur, Giant electrocaloric effect in thin-film $\text{PbZr}_{0.95}\text{Ti}_{0.05}\text{O}_3$, *Science* **311**, 1270 (2006).
- [8] P. Vales-Castro, R. Faye, M. Vellvehi, Y. Nouchokgwe, X. Perpiñá, J. M. Caicedo, X. Jordà, K. Roleder, D. Kajewski, A. Perez-Tomas, E. Defay, and G. Catalan, Origin of large negative electrocaloric effect in antiferroelectric PbZrO_3 , *Phys. Rev. B* **103**, 054112 (2021).
- [9] G. Shirane, E. Sawaguchi, and Y. Takagi, Dielectric properties of lead zirconate, *Phys. Rev.* **84**, 476 (1951).
- [10] E. Sawaguchi, H. Maniwa, and S. Hoshino, Antiferroelectric structure of lead zirconate, *Phys. Rev.* **83**, 1078 (1951).
- [11] G. Shirane and R. Pepinsky, Phase transitions in antiferroelectric PbHfO_3 , *Phys. Rev.* **91**, 812 (1953).
- [12] M.-H. Zhang, L. Fulanović, C. Zhao, and J. Koruza, Review on field-induced phase transitions in lead-free NaNbO_3 -based antiferroelectric perovskite oxides for energy storage, *Journal of Materiomics* **9**, 1 (2023).
- [13] J. Gao, Q. Li, S. Zhang, and J.-F. Li, Lead-free antiferroelectric AgNbO_3 : Phase transitions and structure engineering for dielectric energy storage applications, *J. Appl. Phys.* **128**, 070903 (2020).
- [14] P. Goudochnikov and A. J. Bell, Correlations between transition temperature, tolerance factor and cohesive energy in 2+4+ perovskites, *J. Phys.: Condens. Matter* **19**, 176201 (2007).
- [15] R. D. Shannon, Revised effective ionic radii and systematic studies of interatomic distances in halides and chalcogenides, *Acta Crystallogr.* **32**, 751 (1976).
- [16] I. D. Brown, *The Chemical Bond in Inorganic Chemistry: The Bond Valence Model* (Oxford University Press, 2016).
- [17] A. M. Glazer, K. Roleder, and J. Dec, Structure and disorder in single-crystal lead zirconate, PbZrO_3 , *Acta Crystallogr. B* **49**, 846 (1993).
- [18] X. Tan, C. Ma, J. Frederick, S. Beckman, and K. G. Webber, The antiferroelectric \leftrightarrow ferroelectric phase transition in lead-containing and lead-free perovskite ceramics, *J. Am. Ceram. Soc.* **94**, 4091 (2011).
- [19] J. S. Baker, M. Paściak, J. K. Shenton, P. Vales-Castro, B. Xu, J. Hlinka, P. Márton, R. G. Burkovsky, G. Catalan, and A. M. Glazer, A re-examination of antiferroelectric PbZrO_3 and PbHfO_3 : An 80-atom *Pnam* structure, [arXiv:2102.08856](https://arxiv.org/abs/2102.08856).
- [20] H. Aramberri, C. Cazorla, M. Stengel, and J. Íñiguez, On the possibility that PbZrO_3 not be antiferroelectric, *npj Comput. Mater.* **7**, 196 (2021).
- [21] N. A. Benedek and C. J. Fennie, Why are there so few perovskite ferroelectrics? *J. Phys. Chem. C* **117**, 13339 (2013).
- [22] V. V. Lemanov, A. V. Sotnikov, E. P. Smirnova, M. Wehnacht, and R. Kunze, Perovskite CaTiO_3 as an incipient ferroelectric, *Solid State Commun.* **110**, 611 (1999).
- [23] D. J. Singh, Structure and energetics of antiferroelectric PbZrO_3 , *Phys. Rev. B* **52**, 12559 (1995).
- [24] S. Saha, T. P. Sinha, and A. Mookerjee, First principles study of electronic structure and optical properties of CaTiO_3 , *Eur. Phys. J. B* **18**, 207 (2000).
- [25] A. K. Tagantsev, K. Vaideswaran, S. B. Vakhrushev, A. V. Filimonov, R. G. Burkovsky, A. Shaganov, D. Andronikova, A. I. Rudskoy, A. Q. R. Baron, H. Uchiyama, D. Chernyshov, A. Bosak, Z. Ujma, K. Roleder, A. Majchrowski, J. H. Ko, and N. Setter, The origin of antiferroelectricity in PbZrO_3 , *Nat. Commun.* **4**, 2229 (2013).
- [26] J. Hlinka, T. Ostapchuk, E. Buixaderas, C. Kadlec, P. Kuzel, I. Gregora, J. Kroupa, M. Savinov, A. Klic, J. Drahokoupil, I. Etxebarria, and J. Dec, Multiple soft-mode vibrations of lead zirconate, *Phys. Rev. Lett.* **112**, 197601 (2014).
- [27] J. Íñiguez, M. Stengel, S. Prosandeev, and L. Bellaiche, First-principles study of the multimode antiferroelectric transition in PbZrO_3 , *Phys. Rev. B* **90**, 220103(R) (2014).
- [28] K. Patel, S. Prosandeev, Y. Yang, B. Xu, J. Íñiguez, and L. Bellaiche, Atomistic mechanism leading to complex

- antiferroelectric and incommensurate perovskites, *Phys. Rev. B* **94**, 054107 (2016).
- [29] K. Shapovalov and M. Stengel, Tilt-driven antiferroelectricity in PbZrO_3 , *Phys. Rev. Mater.* **7**, L071401 (2023).
- [30] X. Gonze, B. Amadon, G. Antonius, F. Arnardi, L. Baguet, J.-M. Beuken, J. Bieder, F. Bottin, J. Bouchet, E. Bousquet, N. Brouwer, F. Bruneval, G. Brunin, T. Cavignac, J.-B. Charraud, W. Chen, M. Côté, S. Cottenier, J. Denier, G. Geneste *et al.*, The ABINIT project: Impact, environment and recent developments, *Comput. Phys. Commun.* **248**, 107042 (2020).
- [31] X. Gonze, F. Jollet, F. Abreu Araujo, D. Adams, B. Amadon, T. Applencourt, C. Audouze, J.-M. Beuken, J. Bieder, A. Bokhanchuk, E. Bousquet, F. Bruneval, D. Caliste, M. Côté, F. Dahm, F. Da Pieve, M. Delaveau, M. Di Gennaro, B. Dorado, C. Espejo, G. Geneste, L. Genovese, A. Gerossier, M. Giantomassi *et al.*, Recent developments in the ABINIT software package, *Comput. Phys. Commun.* **205**, 106 (2016).
- [32] X. Gonze, B. Amadon, P.-M. Anglade, J.-M. Beuken, F. Bottin, P. Boulanger, F. Bruneval, D. Caliste, R. Caracas, M. Côté, T. Deutsch, L. Genovese, Ph. Ghosez, M. Giantomassi, S. Goedecker, D. R. Hamann, P. Hermet, F. Jollet, G. Jomard, S. Leroux, M. Mancini, S. Mazevet *et al.*, ABINIT: First-principles approach to material and nanosystem properties, *Comput. Phys. Commun.* **180**, 2582 (2009).
- [33] X. Gonze, J.-M. Beuken, R. Caracas, F. Detraux, M. Fuchs, G.-M. Rignanese, L. Sindic, M. Verstraete, G. Zerah, F. Jollet, M. Torrent, A. Roy, M. Mikami, Ph. Ghosez, J.-Y. Raty, and D. C. Allan, First-principles computation of material properties: The ABINIT software project, *Comput. Mater. Sci.* **25**, 478 (2002).
- [34] M. J. van Setten, M. Giantomassi, E. Bousquet, M. J. Verstraete, D. R. Hamann, X. Gonze, and G.-M. Rignanese, The PseudoDojo: Training and grading a 85 element optimized norm-conserving pseudopotential table, *Comput. Phys. Commun.* **226**, 39 (2018).
- [35] D. R. Hamann, Optimized norm-conserving Vanderbilt pseudopotentials, *Phys. Rev. B* **88**, 085117 (2013).
- [36] J. P. Perdew, A. Ruzsinszky, G. I. Csonka, O. A. Vydrov, G. E. Scuseria, L. A. Constantin, X. Zhou, and K. Burke, Restoring the density-gradient expansion for exchange in solids and surfaces, *Phys. Rev. Lett.* **100**, 136406 (2008).
- [37] Z. Wu and R. E. Cohen, More accurate generalized gradient approximation for solids, *Phys. Rev. B* **73**, 235116 (2006).
- [38] M. M. Schmitt, *First- and Second-Principles Studies of Perovskites*, Ph.D. dissertation, Université de Liège, 2020.
- [39] See Supplemental Material at <http://link.aps.org/supplemental/10.1103/PhysRevB.108.L140304> for the impact of different exchange-correlation functionals, structural relaxations with fixed lattice parameters, phonon dispersions by replacing the atomic masses, effects of modifying IFCs on phonon dispersions, and effects of modifying the anharmonic interactions.
- [40] X. Gonze and C. Lee, Dynamical matrices, Born effective charges, dielectric permittivity tensors, and interatomic force constants from density-functional perturbation theory, *Phys. Rev. B* **55**, 10355 (1997).
- [41] J. C. Wojdeł, P. Hermet, M. P. Ljungberg, P. Ghosez, and J. Íñiguez, First-principles model potentials for lattice-dynamical studies: general methodology and example of application to ferroic perovskite oxides, *J. Phys.: Condens. Matter* **25**, 305401 (2013).
- [42] C. Escorihuela-Sayalero, J. C. Wojdeł, and J. Íñiguez, Efficient systematic scheme to construct second-principles lattice dynamical models, *Phys. Rev. B* **95**, 094115 (2017).
- [43] A. Togo and I. Tanaka, First principles phonon calculations in materials science, *Scr. Mater.* **108**, 1 (2015).
- [44] Ph. Ghosez, E. Cockayne, U. V. Waghmare, and K. M. Rabe, Lattice dynamics of BaTiO_3 , PbTiO_3 , and PbZrO_3 : A comparative first-principles study, *Phys. Rev. B* **60**, 836 (1999).
- [45] D. Amoroso, A. Cano, and P. Ghosez, First-principles study of $(\text{Ba}, \text{Ca})\text{TiO}_3$ and $\text{Ba}(\text{Zr}, \text{Ti})\text{O}_3$ solid solutions, *Phys. Rev. B* **97**, 174108 (2018).
- [46] R. E. Cohen, Origin of ferroelectricity in perovskite oxides, *Nature (London)* **358**, 136 (1992).
- [47] A. Walsh, D. J. Payne, R. G. Egdell, and G. W. Watson, Stereochemistry of post-transition metal oxides: Revision of the classical lone pair model, *Chem. Soc. Rev.* **40**, 4455 (2011).